

Unsupervised Restoration of Hair- Occluded Lesion in Dermoscopic Images

Damilola A. Okuboyejo¹
okuboyejoda@tut.ac.za

Oludayo O. Olugbara²
oludayoo@dut.ac.za

Solomon A. Odunaike¹
odunaikesa@tut.ac.za

¹Department of Software
Engineering, Tshwane University
of Technology, South Africa.

²Department of Information
Technology, Durban University of
Technology, South Africa.

Abstract

The presence of artefacts such as hair shaft, thin blood vessel, ruler marking and air bubble in medical images makes the diagnosis of skin-related medical images very difficult. This paper uses a two-stage artefact detection termed Fast Image Restoration (FIR) via Canny algorithm and Line Segment Detection (LSD) operation for effective detection of artefacts. The Fast Marching Method (FMM) was applied at each stage for the removal of artefacts from a dermoscopic image in an unsupervised environment while ensuring morphological features of the lesion areas of the image data are preserved. Statistical Analysis performed to determine the accuracy of artefact recognition and repair validation of our method yields a Sensitivity of 98.27%, Specificity of 93.75% and Diagnostic Accuracy of 96.10%. These results indicate that our method gives an acceptable level of accuracy.

1 Introduction

Melanoma, which is currently the third prevalent cancer in some parts of the world were for instance reported to occur in 61.7 for every 100000 Australian men and 40.0 for every 100000 Australian women [1]. The development of automated diagnosis systems, capable of performing some level of remote diagnosis of skin cancer diseases such as melanoma and basal cell carcinoma and equally assisting physicians in various imaging task has gained tremendous attention in the bioinformatics and computer vision research [2]. The efforts towards automation of diagnosis procedures are mainly geared to improve the speed of diagnosis and to increase the reproducibility of results. The automated diagnosis has also helped in reducing first-time diagnosis error which sometimes could be as much as 40% [3, 4]. The presence of artefacts such as hair shaft, thin blood vessel, ruler marking and air bubbles in the medical imaging vision makes the diagnosis of skin-related medical imaging very difficult [5-7].

It is important therefore, to mitigate these challenges while still ensuring that quality and time-effective diagnosis can be achieved at a reasonable speed. A popular approach in the literature proposed by Lee [8] is DullRazor hair removal that uses a Top-Hat grayscale morphological closing operation to smoothen out low intensity data of thick dark hairs. The apparent challenge to most of the current effort is the limitation in detecting and repairing

thin hair structures while concurrently preserving the morphological features of the image data. The high computational resources required by most of these techniques also presents a challenge.

This study proposes an approach using bilateral filter and a two-stage artefact detection termed Fast Image Restoration (FIR) via Canny algorithm [9] and Line Segment Detection (LSD) [10] operation with fast marching inpainting method in the attempt to autotomize hair occluded artefacts from dermoscopic image in an unsupervised environment while concurrently preserving the morphological features of the lesion image.

2 Materials and Methods

2.1 Algorithm

The following algorithm is applied in this study for unsupervised restoration of Hair-occluded lesion in a dermoscopic image.

Step 1: Input dermoscopic image in RGB colour space.

Step 2: Bilateral filtering [11] to perform edge-preserving smoothing operation on the lesion image in a CIE L*a*b space.

Step 3: First-level hair-shaft and ruler marking detection using Canny operator [9] with Gaussian filtering and Progressive Probabilistic Hough Transform [12] on result of step 2.

Step 4: Apply Fast Marching inpainting Method (FMM) [13].

Step 5: Dilate with kernel $k_{2 \times 2}$ in CIE L*a*b space to remove noise.

Step 6: Second-level hair-shaft and ruler marking using a Line segmentation operator.

Step 7: Re-applied fast marching inpainting.

Step 8: Dilate again with kernel $k_{2 \times 2}$ in CIE L*a*b space to remove salient salty noise.

2.2 Image Standardization

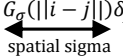
In our experiments, we discovered that CIE*Lab produced a convincing result when compared to its counterparts (CIE L*u*v and CIE X*Y*Z) and the popular YCbCr colour space. This would also help to avoid device dependency requirement of RGB colour space.

2.3 Filtering Techniques

2.3.1 Gaussian Filter

The Gaussian filter was used to compute the weighted mean of pixels, while being independent of image resolution and spatial location. One major challenge noticed with the use of Gaussian filter is that edge preservation, which is required in detection of the Hair-shaft was an issue [see Figure 1(a), 1(c) and 1(d)].

$$\text{Gaussian Filter } G(\delta)_i = \sum_{j \in S} G_{\sigma}(\|i - j\|) \delta_j \quad \text{Eq 1}$$



The problem above is caused by averaging of edges caused by the filters. Bilateral filtering or Diffusion could be used to resolve this challenge.



Figure 1(a) - Original



Figure 1(b) - Bilateral

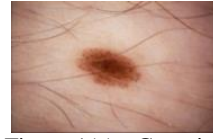


Figure 1(c) - Gaussian



Figure 1(d) - Median

In this study, we applied the Bilateral filtering because of its non-iterative nature and to ensure that smoothing does not stop at thin lines as seen in Anisotropic Diffusion.

2.3.2 Bilateral Filter

The Bilateral filtering technique combines both range and domain filters. The traditional low-pass filters perform domain filtering and enforce closeness (neighbourhood in the domain) by weighting pixel values with coefficients that fall off with distance [11]. In contrast, the bilateral filter computes range filtering in addition to domain filtering. When smoothing an image, preservation of edges can be achieved by combining range filtering by domain filtering [see Figure 1(a) and Figure 1(b)]. Our implementation of domain filtering used is according to Gaussian filter [see Eq 1].

$$\text{Gray Images: } B\langle\delta\rangle_{i_g} = \beta^{-1} \sum_{j_g \in S} \underbrace{G_{\sigma_s}(|i_g - j_g|)}_{\text{domain sigma}} \underbrace{G_{\sigma_r}(|i_g - j_g|)}_{\text{range sigma}} \delta_{j_g} \quad \text{Eq 2}$$

$$\text{Colored Images: } B\langle\delta\rangle_{i_c} = \beta^{-1} \sum_{j_c \in S} \underbrace{G_{\sigma_s}(|i_c - j_c|)}_{\text{domain sigma}} \underbrace{G_{\sigma_r}(|i_c - j_c|)}_{\text{range sigma}} \delta_{j_c} \quad \text{Eq 3}$$

β^{-1} is the normalization factor

$|i_g - j_g|$ is the intensity changes

$|i_c - j_c|$ is the color difference in either RGB or CIE $L^*a^*b^*$

δ_{j_g} and δ_{j_c} represents scalar and 3D vector quantity respectively

2.4 Dilation Morphological Operation

In relation to mathematical morphology, dilation provide a maximizing operation technique for causing bright regions within an image to grow, thus leading to removal of salient noise. It works by convolving an image δ with a structuring element (kernel) κ of any shape or size.

$$\delta \oplus \kappa = \bigcup (\kappa + l; l \in \delta) \quad \text{Eq 4}$$

2.5 Artefact Recognition

2.5.1 Progressive Probabilistic Hough Transform

The Progressive Probabilistic Hough Transform (PPHT) was applied to estimate hair-shafts and ruler marking based on the result of the Canny edge [see Figure 2(c) - 2(e)]. The PPHT performs line segmentation by using the difference in the fraction of votes needed to effectively detect lines with different numbers of supporting points resulting from operators such as Sobel and Canny.

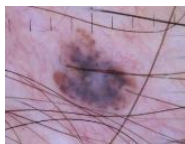


Figure 2(a) - source image

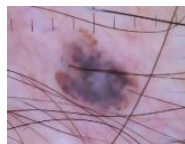


Figure 2(b) - filtered image



Figure 2(c) - canny edge



Figure 2(d) - mask from PPHT

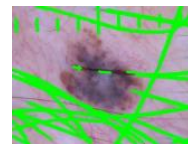


Figure 2(e) - line segment by PPHT

2.5.2 Fast Marching Inpainting

Inpainting generally involves using textures and colours identical to a defined boundary of an identified gap to fill different regions in the gap defined by contour lines. We applied the Fast Marching Methods (FMM) proposed by Talea [13] as highlighted in the pseudo code below.

Let δ represent an image having gradient g , such that
 $\delta_i = \text{pixel value of image } \delta \text{ at } i_{x,y}$
 $\delta_j = \text{pixel value of image } \delta \text{ at } j_{x,y}$
 $g_i = \text{gradient value of } \delta_i$; $g_j = \text{gradient value of } \delta_j$

if \mathcal{D} represent First Order Approximation (FDA), such that

$\mathcal{D}_i = \text{FDA of } \delta_i$
 $\mathcal{D}_j = \text{FDA of } \delta_j$

then, it follows that

$\mathcal{D}_i = \delta_j + g_j(i - j)$

let $\mathcal{N}_{z_i} = \text{neighborhood pixel of size } z \text{ of the known image around } i$

$\beta_{i,j} = \text{weighted function to propagate sharp image details to inpainted arena}$

if \mathfrak{R} represent region to be inpainted

\mathbb{B} represent boundary of the region

\mathfrak{R}_i represent initial position in the region

ξ_i represent inpaint point i ; $\xi_i = \frac{\sum_{j \in \mathcal{N}_{z_i}} \beta_{i,j} \mathcal{D}_j}{\sum_{j \in \mathcal{N}_{z_i}} \beta_{i,j}}$

Eq 5

While (\mathbb{B} still contains valid points)

$i = \text{pixel } \varphi \text{ nearest to } \mathfrak{R}_i$

perform interpolation on i using Eq 5

advance \mathbb{B} into \mathfrak{R}

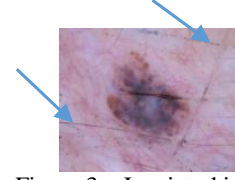


Figure 3 – Inpainted image after applying FMM

While the combination of Bilateral filtering, Canny operation and PPHT using well-defined hysteresis threshold achieved a level of success, a thorough detection of the noise was not performed [see sample arrows drawn in Figure 3]. This challenge was addressed by performing a second-level artefact recognition using the line segmentation operator.

2.5.3 Line Segment Detector

We applied the LSD technique on results produced by FMM [see Figure 3] and generated edge points for the remaining hair-shafts as highlighted in Figure 4(a). The mask of Figure 4(a) was obtained and used by FMM to perform a second-level inpainting that resulted in Figure 4(c). In this paper, we followed the recommendations by Gioi et al.[10] considering our objectives. The approach proposed in [10] is based on [14, 15] and Desolneux's line validation method [16] using Helmholtz principle [17].

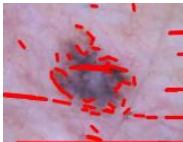


Figure 4(a) – line segment by LSD



Figure 4(b) – LSD mask

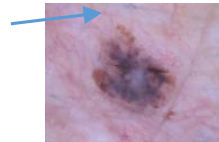


Figure 4(c) – result after applying FMM



Figure 4(d) – morphologically dilated image

While the result in Figure 4(c) looks promising, some artefacts as pointed out by the arrows were still noticeable. Morphological dilation was performed on Figure 4(c) to remove the salient salty noise and this resulted in output in Figure 4(d).

3 Results and Discussions

Our method has been applied to a dataset¹ of a total of 299 images. A total of 294 of the images are melanocytic lesion bound and 5 are non-melanocytic. Out of the 294 melanocytic images, 105 images were already histopathologically certified by the Dermatologists as melanoma and the remaining 189 images as being benign naevus. The ground truth of the artefacts was obtained from manual identification and sketch-trace of the visible artefacts in a given image.

The implementation of each step in the highlighted algorithm of section 2.1 was computed on a virtual machine running Ubuntu 12.0.4.3 LTS, with base memory of 3096MB and 2 processors. The machine has VT-X/AMD-V hardware virtualization capability with nested paging. Average speed of execution of the complete algorithm is 380ms.

In order to ensure that hair-shaft, including fine hairs and other related artefacts are well recognized, the first part of our approach is centred on smoothening of each image while retaining the edges of artefacts to be repaired. Our study indicates that the best filtering technique for our objective is bilateral filter [see Figure 1(a) – 1(d)]. The second part of our approach is focused on identification of artefacts in a given lesion using a two-stage detection process of the Canny operator with PPHT and line segment detector in that order. A remarkable result was achieved in our study because of the use of both Canny and LSD, rather than using only either of them. It is important therefore to state that applying the Canny operator with PPHT before LSD produced a better result than the reverse.

The statistical analysis based on the metrics of Sensitivity, Specificity and Diagnostic Accuracy was used to determine the performance of artefact recognition and repair validation. Our proposed approach reports a true positive rate (Sensitivity) of 98.27% and a true negative rate (Specificity) of 93.75%. The diagnostic accuracy achieved is recorded at level high of 96.10%. Figure 5(a) – Figure 5(d) and Figure 6(a) – Figure 6(d) highlight a comparable output of our approach with that of DullRazor [8] and Zhou et al. [7].

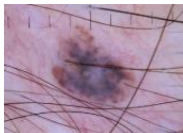


Figure 5(a) – Original Image

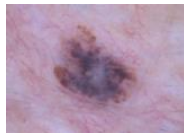


Figure 5(b) – DullRazor

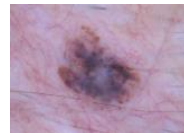


Figure 5(c) – Zhou



Figure 5(d) – Our approach

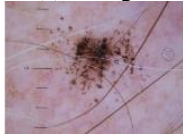


Figure 6(a) – Original Image



Figure 6(b) – DullRazor



Figure 6(c) – Zhou

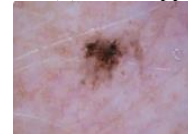


Figure 6(d) – Our approach

4 Conclusion

We proposed in this study a fast and effective approach towards repairing hair-occluded and other artefacts in a dermoscopic images. The artefact recognition involved a two-stage process of using Canny and LSD operator. Experimental results indicate our proposed approach is dependable, robust and can effectively repair lesions occluded with hair-shafts and air bubbles. Dermatologists can easily use our approach as a form of pre-processing of dermoscopic images before lesion segmentation and classification. Our approach worked well on various types of lesion as described in section 3.

¹ The images were provided as a support in part by Dermatology Society of South Africa (DSSA).

References

- [1] Australian Institute of Health and Welfare & Australian Association of Cancer Registries 2012, Cancer in Australia, in, 2012.
- [2] R. Dobrescu, M. Dobrescu, S. Mocanu, D. Popescu, Medical images classification for skin cancer diagnosis based on combined texture and fractal analysis. Proceedings of WSEAS Transactions on Biology and Biomedicine; 2010. July 2010.
- [3] M. Kantrowitz. Pathology Reports May Contain Errors. 2009. Available from: <http://www.kantrowitz.com/cancerpoints/diagnosiserrors.html> (Accessed Jan 16th, 2014).
- [4] H. Singh, S. Sethi, M. Raber, L.A. Petersen, Errors in Cancer Diagnosis: Current Understanding and Future Directions, JCO, (2007) 5009-5018.
- [5] Q. Abbas, I.F. García, M. Rashid, Unsupervised skin lesions border detection via two-dimensional image analysis, Comput Methods Program Biomed, (2010).
- [6] A.K. Mitra, R. Parekh, Automated detection of skin disease using texture features, International Journal of Engineering Science and Technology, 3 (2011).
- [7] H. Zhou, M. Chen, R. Gass, J.M. Rehg, L. Ferris, J. Ho, L. Drogowski, Feature Preserving Artifact Removal from Dermoscopy Images. Proceedings of SPIE Medical Imaging: Image Processing; 2008. San Diego, USA.
- [8] K.T. Lee, R. Galagher, A. Coldman, D. Mclean, Dullrazor: A software approach to hair removal from images, Comput Biol Med, 27 (1997) 533-543.
- [9] J. Canny, A Computational Approach to Edge Detection, IEEE Transactions on Pattern Analysis and Machine Intelligence, Vol PAM 1-8, No 6. (1986).
- [10] R.G.v. Gioi, J. Jakubowicz, J.-M. Morcel, G. Randall, LSD: A Line Segment Detector, Image Processing On Line, (2012).
- [11] C. Tomasi, R. Manduchi, Bilateral Filtering for Gray and Color Images. Proceedings of IEEE International Conference on Computer Vision; 1998. Bombay, India.
- [12] J. Matas, C. Galambos, J. Kittler, Robust Detection of Lines Using the Progressive Probabilistic Hough Transform, Computer Vision and Image Understanding, 78 (2000) 119-137.
- [13] A.C. Talea, An Image Inpainting Technique based on the Fast Marching Method, Journal of Graphics Tools, Vol 9. No. 1 (2004) 25-36.
- [14] J.B. Burns, A.R. Hanson, E.M. Riesenman, Extracting Straight Lines, IEEE Transactions on Pattern Analysis and Machine Intelligence, vol. 8, no. 4 (1986) 425-455.
- [15] J.R. Beveridge, C. Graves, C. Leshner, Some Lessons learned from Coding the Burns Line Extraction Algorithm in the Darpa Image Understanding Environment, Technical Report CS-96-125C.S. Department, Colorado State University, 1996. Available from: <http://www.cs.colostate.edu/TechReports/Reports/1996/tr96-125.pdf> (Accessed: February 2, 2014).
- [16] A. Desolneux, L. Moisan, J.-M. Morel, Meaningful Alignments, International Journal of Computer Vision, vol. 40, no. 1 (2000) 7-23.
- [17] A. Desolneux, L. Moisan, J.-M. Morel, From Gestalt Theory to Image Analysis - A Probabilistic Approach, International Applied Mathematics, vol. 34 (2008).